Quantitative imaging of gene-expressing liposomes reveals rare favorable phenotypes

Blanken, Duco; van Nies, Pauline; Danelon, Christophe

DOI
10.1088/1478-3975/ab0c62

Publication date
2019

Document Version
Final published version

Published in
Physical Biology

Physical Biology

OFFICIAL JOURNAL OF
Sociedad de Biofísicos Latino Americanos

PAPER

Quantitative imaging of gene-expressing liposomes reveals rare favorable phenotypes

To cite this article: Duco Blanken *et al* 2019 *Phys. Biol.* **16** 045002

Physical Biology

PAPER

Quantitative imaging of gene-expressing liposomes reveals rare favorable phenotypes

Duco Blanken[1], Pauline van Nies[1] and Christophe Danelon[1,2]

[1] Department of Bionanoscience, Kavli Institute of Nanoscience, Delft University of Technology, van der Maasweg 9, 2629 HZ, Delft, The Netherlands
[2] Author to whom any correspondence should be addressed.

E-mail: c.j.a.danelon@tudelft.nl

RECEIVED
12 December 2018

REVISED
22 February 2019

ACCEPTED FOR PUBLICATION
4 March 2019

PUBLISHED
12 April 2019

Keywords: synthetic cell, minimal cell, PURE system, cell-free gene expression, liposome

Supplementary material for this article is available online

Abstract

The biosynthesis of proteins from genomic DNA is a universal process in every living organism. Building a synthetic cell using separate biological parts hence implies to reconstitute a minimal gene expression apparatus and to compartmentalize it in a cell-mimicking environment. Previous studies have demonstrated that the PURE (Protein synthesis Using Recombinant Elements) system could be functionally encapsulated inside lipid vesicles. However, quantitative insights on functional consequences of spatial confinement of PURE system reactions remain scarce, which has hampered the full exploitation of gene-expressing liposomes as the fundamental unit to build an artificial cell. We report on direct imaging of tens of thousands of gene-expressing liposomes per sample allowing us to assess sub-population features in a statistically relevant manner. Both the vesicle size (diameter $<10\ \mu$m) and lipid composition (mixture of phospholipids with zwitterionic and negatively charged headgroups, including cardiolipin) are compatible with the properties of bacterial cells. Therefore, our liposomes provide a suitable chassis to host the *Escherichia coli*-derived PURE translation machinery and other bacterial processes in future developments. The potential of high-content imaging to identify rare phenotypes is demonstrated by the fact that a subset of the liposome population exhibits a remarkably high yield of synthesized protein or a prolonged expression lifespan that surpasses the performance of ensemble liposome-averaged and bulk reactions. Among the three commercial PURE systems tested, PURE*frex*2.0 offers the most favorable phenotypes displaying both high yield and long protein synthesis lifespan. Moreover, probing membrane permeability reveals a large heterogeneity amongst liposomes. *In situ* expression and membrane embedding of the pore-forming connexin leads to a characteristic permeability time profile, while increasing the fraction of permeable liposomes in the population. We see diversity in gene expression dynamics and membrane permeability as an opportunity to complement a rational design approach aiming at further implementing biological functions in liposome-based synthetic cells.

Introduction

Compartmentalization of cell-free protein synthesis has emerged as a scaffold to build a whole (semi) synthetic cell following a bottom-up approach [1–6]. Encoding functions onto genomic DNA [6] or RNA [7, 8] provides a unique route to self-replication of the core machinery as alternative approaches relying exclusively on purified proteins and RNAs are unavoidably destined to death by dilution upon division events. This gene-directed strategy comes with a great system's complexity since the entire gene expression network itself comprises about hundred different components in its minimal form [9, 10]. An example of minimal gene expression platform is the PURE (protein synthesis using recombinant elements) system, an *E. coli*-based *in vitro* transcription-translation (IVTT) system [9, 10]. Its utilization in the context of building a minimal synthetic cell is particularly suited as it bypasses the endogenous complexity of cell lysates, thereby channeling resources (energy-rich phosphate donor

molecule, nucleoside triphosphates and amino acids) for gene expression-related processes only. PURE system reaction kinetics have been monitored under a variety of initial conditions using different fluorescent reporters of mRNA and synthesized protein (see our accompanying paper [11] and references therein).

Various types of cell-like compartments have been proposed to enclose the biosynthesis apparatus, such as phospholipid vesicles (called liposomes) [1–6, 12], water-in-oil emulsion droplets [7, 13], peptide [14] and polymersome vesicles [15]. In particular, spatial confinement of gene expression systems inside liposomes provides a chassis that closely emulates the bacterial cytoplasmic environment. The mechanical properties of the phospholipid bilayers can be exploited to mimic cellular processes, e.g. membrane deformation and subsequent compartment division [16]. Moreover, the lipid membrane can serve as a native-like platform to integrate proteins and regulate the ionic and molecular exchanges with the environment [3, 17–20]. Finally, recent progress on *in vitro* phospholipid synthesis by reconstituted bacterial enzymes represents an encouraging step towards liposome growth through internal production of its membrane constituents [5, 21, 22]. Hence, we postulate that liposome-based compartments are uniquely suited to recapitulate biological functions in synthetic cell research.

We identify three important requirements to develop a robust in-liposome gene expression platform, which will serve as a scaffold to further implement cellular functionalities. (i) One needs a predictive model describing the kinetics of mRNA and protein synthesis from single and multiple genes, as well as the key factors that govern performance ([11] and references therein). (ii) Liposome preparation methods need to be compatible with a large variety of lipids (e.g. scaffolding, signaling, membrane remodeling active lipids) and they should not alter the biological integrity of the entrapped compounds or the mechanical properties of the membrane. Moreover, the methods should generate cell-sized ($1\ \mu m <$ diameter $< 10\ \mu m$) unilamellar vesicles at a yield enabling high-throughput quantitative analysis of gene expression dynamics at the single liposome level. (iii) The new system's properties associated with liposome compartmentalization should be apprehended and harnessed. These include compositional heterogeneity or stochastic effects arising from low-copy number of some reactants [23–27], possible interaction with the lipidic surface [13], macromolecular crowding [28–30], effects of confinement on reaction rates [31], and membrane permeability governing molecular exchange with the external environment [3].

In this work, we established a robust protocol for preparing PURE system-containing liposomes. The method was applied to all three commercially available PURE system variants, i.e. PURExpress, PURE*frex* and PURE*frex*2.0 (see our accompanying paper [11] for details on their composition and bulk reaction properties). Gene expressing liposomes with sizes and lipid composition relevant to bacterial cell physiology have been produced at high yield and immobilized for long-term (>12 h) time-lapse fluorescence imaging of the yellow fluorescent protein (YFP) reporter. A disparity in translation kinetics and end-point protein levels between liposomes within a population has previously been observed [4, 12, 23, 26, 27, 32] and theoretically predicted [33] (for a recent review, see [34]). The high-content liposome analysis performed here unravels new quantitative insights on stochastic enhancement and on production differences between the three types of PURE system.

Previous attempts to regulate the molecular exchange between the liposome interior and its environment (requirement (iii)) utilized membrane-spanning protein channels or transporters, such as α-hemolysin [3], MScL [18], connexin [17, 19] and EmrE [20], exploited transient bilayer defects [4, 23] or mild detergent at sub-solubilizing concentration [35]. Stable permeability with pore forming proteins could potentially alleviate the problem of energy and nutrient shortage inherent to sealed liposomes, with the promise of sustained gene expression [3]. We found an intrinsic heterogeneity of membrane permeability, demonstrated by the fact that liposomes coexisting in the same population take up, or not, a fluorescent dye with slightly larger size than relevant IVTT nutrients. We then expressed inside liposomes the connexin Cx43, a protein channel with a molecular mass cutoff of about 1.5 kDa [36], which is suitable for selective translocation of low-molecular weight substances. We showed that internal production of Cx43 does not lower expression of a second gene coding for YFP. Interestingly, functional reconstitution of Cx43 leads to distinct permeability kinetics with a sharp increase after about 60 min expression. However, no prominent increase of the YFP yield or translation lifespan could be observed, suggesting that the concentration of permeable nutrients available in the external solution is not limiting PURE*frex* reactions in liposomes.

Materials and methods

DNA constructs

A linear DNA template encoding for the eYFP (enhanced yellow fluorescent protein) was used to enable direct fluorescence readout of the level of synthesized protein [32, 37]. Transcriptional elements include the T7 promoter and terminator, and the eYFP sequence was codon-optimized for expression in the *E. coli*-based PURE system [37]. The encoded Spinach RNA aptamer was not exploited for quantitative analysis of mRNA production (figure S2 (stacks.iop.org/PhysBio/16/045002/mmedia)). Linear DNA constructs were regularly prepared by polymerase chain reaction using a circular plasmid as template, as also described in our accompanying article [11]. The linear Cx43 construct was prepared from a plasmid coding for

the Cx43-eGFP fusion protein [17]. Forward (5′-GCGAAATTAATACGACTCACTATAGGGAGACC-3′) and reverse (5′-CAAAAAACCCCTCAAGACCCGTTTAGAGGCCCCAAGGGGTTATGCTAGTCAGATTTCCAGATCATCAGGACGCG-3′) primers were used to remove the eGFP sequence.

Liposome preparation

To prepare liposomes containing a PURE system reaction mixture, we optimized a method previously described by our lab [4, 5]. The experimental workflow consists of four main steps: (i) preparation of lipid-coated beads, (ii) swelling of the lipid film by gentle rehydration with the PURE system solution, (iii) freeze-thaw cycles to break multilamellar structures and increase encapsulation efficiency, (iv) immobilization of liposomes on a coverslip, followed by triggering and monitoring gene expression by time-lapse fluorescence microscopy.

The lipid mixture deposited on the glass beads (212–300 μm acid washed glass beads, Sigma Aldrich) consists of 1,2-dioleoyl-*sn*-glycero-3-phosphocholine (DOPC), 1,2-dioleoyl-*sn*-glycero-3-phosphatidylethanolamine (DOPE), 1,2-dioleoyl-*sn*-glycero-3-phospho-(1′-*rac*-glycerol) (DOPG), 1′,3′-bis[1,2-dioleoyl-*sn*-glycero-3-phospho]-*sn*-glycerol (cardiolipin), supplemented with 1,2-distearoyl-*sn*-glycero-3-phosphoethanolamine-N-[biotinyl(polyethylene glycol)-2000] (DSPE-PEG-biotin) and Texas Red 1,2-dihexadecanoyl-*sn*-glycero-3-phosphoethanolamine, triethylammonium salt (TR-DHPE). All lipids were from Avanti Polar Lipids, except TR-DHPE that was purchased from Thermo Fisher Scientific. A lipid matrix with oleoyl (18:1) acyl chains and sub-zero phase transition temperature was chosen as it enables natural lipid film swelling on ice, which prevents gene expression from starting. A mixture of 2.54 mg DOPC (50 mol%), 1.68 mg DOPE (36 mol%), 0.58 mg DOPG (12 mol%), 0.20 mg cardiolipin (2 mol%), 0.05 mg DSPE-PEG(2000)-biotin (1 mass%) and 0.025 mg TR-DHPE (0.5 mass%), all dissolved in chloroform, was prepared in a round-bottom flask. The lipid-containing chloroform solution was mixed with 100 mM rhamnose dissolved in methanol in a 2.5 to 1 ratio, corresponding to ten rhamnose molecules per lipid. Then, 1.5 g of glass beads was poured to the lipid-sugar mixture and the solution was subjected to 2 h of rotary evaporation at 200 mbar and room temperature, followed by overnight desiccation, resulting in beads coated with stacked lipid bilayers interspersed with rhamnose. The addition of the hydrophilic sugar rhamnose to the lipid film, combined with the presence of PEG-modified lipids, promotes separation of adjacent bilayers and formation of unilamellar vesicles [5, 38].

PURE*frex* and PURE*frex*2.0 are from GeneFrontier Corporation (Chiba, Japan). PURExpress is from New England Biolabs. PURE*frex*, PURE*frex*2.0 and PURExpress reaction mixtures were prepared in 0.5 ml Eppendorf tubes according to the guidelines provided by the manufacturers. The *yfp* DNA template was supplemented at a concentration of 5 ng μl^{-1} (final concentration 7.4 nM). When indicated, 6.25 ng μl^{-1} of the *Cx43* construct was added. All reactions were supplemented with SUPERase RNAse inhibitor (0.75 U μl^{-1} final, Invitrogen). An amount of lipid-coated beads corresponding to 1.25 mg μl^{-1} was added to the 10 μl PURE system solution. Liposomes were formed by spontaneous swelling of the lipid film for 2 h on ice, during which the samples were regularly subjected to manual tumbling. Four freeze-thaw cycles were finally applied by dipping samples in liquid nitrogen in order to increase liposome unilamellarity and encapsulation efficiency.

Surface immobilization of liposomes

Reaction chambers were custom-made by sandblasting two holes of 5 mm in diameter in a 1 mm thick microscopy slide (Thermo Scientific). A 150 μm thick coverslip (Thermo Scientific) was glued on the microscopy slide with Norland Optical Adhesive 61 (Norland) to cover the holes on one side forming the bottom of the chamber. The sample reservoir was functionalized with 1:1 molar ratio of BSA and BSA-biotin (Thermo Fisher Scientific), and then with Neutravidin (Sigma Aldrich), to tether the biotinylated liposomes [4]. About 2 μl of the liposome solution was carefully pipetted (with a cut tip to avoid damaging the liposomes) in the imaging chamber and diluted with 5 μl of feeding solution consisting of 4:7 vol/vol of PURE*frex* Sol I, PURE*frex*2.0 Sol I or PURExpress A and milliQ supplemented with 83 mg l^{-1} Proteinase K. For permeability assays, 2 μl of milliQ was replaced by an equal volume of the dye Cy5 (stock 20 μM), giving a final concentration of 3.33 μM. The second reservoir was filled with water to saturate the air thereby limiting sample evaporation during incubation and imaging. Chambers were closed using a 0.5 mm thick double-sided adhesive silicone sheet (Life Technologies) and a cover slide, creating an interconnecting air volume, which enables oxygen supply to the reaction.

In-liposome gene expression and image acquisition

Image acquisition was performed using a Nikon A1R Laser scanning confocal microscope (LSCM) equipped with an SR Apo TIRF 100× oil immersion objective. Samples were mounted in a stage preheated to 37 °C and imaged using the laser lines 514 nm (YFP), 561 nm (Texas Red) and 640 nm (Cy5), with appropriate emission filters. The distance between the sample and the objective was adjusted manually in order to equatorially dissect as many liposomes as possible. For kinetics measurements, the liposome sample was mounted in the microscope directly after sealing the chamber. An automated image acquisition protocol was run for at least 6 h, taking an image every 10 min. For end-point measurements, the sample chambers were first incubated overnight at 37 °C

in a plate incubator, before being transferred to the microscope. Several YFP acquisition settings were applied in order to make optimal use of the dynamic range of the detector. Each setting was calibrated individually (see below). Montages of six-by-six fields of view, stitched with 20% overlap, were acquired. For kinetics experiments, gene expression was triggered while liposomes were immobilizing on the surface to minimize the delay time before imaging (about 10 min).

High-throughput image analysis

High-throughput analysis of microscopy images was performed using a custom-made MATLAB (Mathworks) code based on the *flood fill* (imfill.m) algorithm supplied with the MATLAB Image Analysis toolbox. The main steps are illustrated in figure S1. In short, after applying a sharpening filter on the Texas Red image, the *flood fill* algorithm increases the intensity value of dark pixels surrounded by lighter pixels, effectively 'filling up' the liposomes. After subtraction of the original Texas Red image and applying a binary threshold, the resulting image serves as a marker for the liposome lumina (figure S1). To ensure that only liposomes are marked, and not debris or noise, the image is first eroded, and regions that do not satisfy the following criterion are dismissed:

$$0.5 < \frac{P^2}{4\pi A} < 2 \tag{1}$$

where P is the perimeter of the region-of-interest (ROI) and A the area. This criterion is established to only select circle-like shapes. The resulting marker is used to identify pixels corresponding to liposome lumina in the YFP and Cy5 channels. The average intensity value of each region is measured in both channels. In the case of YFP the intensity is converted to concentration (see below). In the case of Cy5, this intensity value is normalized by dividing by the Cy5 fluorescence of five randomly selected extra-liposomal ROI's per field of view. For analysis of time-lapse images, the lumen of individual liposomes was traced manually using Fiji [39], and the average fluorescence intensity in both YFP and Cy5 channels was recorded at every time point.

The radius of each liposome in micrometer is estimated as:

$$R = 0.25 \times \left(2 + \sqrt{\frac{3A}{2\pi}}\right) \tag{2}$$

where A is the area of the liposome cross-section in pixel. The area is multiplied by a factor of 3/2 to account for an underestimation by non-equatorial dissection of the liposomes (supplementary text). A value of two pixels is added in order to account for the discrepancy in size between marker and liposome lumen as a result of erosion. To convert pixel values into micrometers, the conversion factor of 0.25 μm/pixel specific to the imaging setup is applied.

Phenomenological fitting of gene expression kinetics

Measured YFP expression kinetics from single liposomes were fit with a phenomenological model to estimate salient dynamic parameters, such as the final yield, YFP production rate and translation lifespan (or time to plateau). The following sigmoid equation was used [40]:

$$y = k' + k\frac{t^n}{t^n + K^n} \tag{3}$$

where t is the time in minutes, y the YFP concentration at a given time point, and k', k, K and n are fit parameters. Using this expression, the final yield corresponds to k and the plateau time—or expression lifespan—(not corrected for the maturation time [11, 37]) is expressed as:

$$T_{\text{plateau}} = \frac{2K}{n} + K. \tag{4}$$

The apparent translation rate, which is defined as the steepness at time $t = K$, is:

$$\text{rate} = \frac{kn}{4K}. \tag{5}$$

Note that these observed kinetic parameters do not account for the synthesis of non-fluorescent products.

Calibration of YFP fluorescence intensity into protein concentration

Conversion formulas that relate microscopy fluorescence to YFP concentrations were obtained via a two-step process. First, a bulk PURExpress reaction with the *yfp* DNA construct was run overnight. A dilution series of the end-point PURE system reaction solution was performed by addition of buffer (20 mM HEPES, 180 mM potassium glutamate, 14 mM magnesium acetate, pH 7.6). For every dilution sample, YFP fluorescence was measured in a spectrophotometer (Cary Eclipse from Agilent, exc/em 515/528 nm), using a 20 μl quartz cuvette (Hellma) at 37 °C. Owing to a previously established conversion factor [11, 37], the final concentration of synthesized YFP can be determined. The same samples were measured by LSCM under conditions (chamber, settings) identical to those employed for liposome experiments. A YFP fluorescence-to-concentration conversion factor could be derived for each laser power setting used. To correct for significant fluctuations of laser power over the period of this study, regular calibration was performed.

Fluorescence intensity thresholds were determined with Fiji [39] to classify liposomes as expressing (with YFP) or permeable (with Cy5). For YFP, the background fluorescence intensity values of sixty randomly selected ROI's outside liposomes from six independent experiments were measured at various laser power settings. The threshold value below which the YFP signal within liposomes was considered negligible

was defined as the mean plus two standard deviations of the calculated background intensity value. This calibration was repeated several times and slightly different threshold values were obtained. Similarly, the Cy5 background intensity value was determined and used for normalization of the liposome intensity values. Liposomes with a normalized Cy5 signal below 0.75 were considered empty (impermeable).

Flow cytometry

Liposomes containing PURE*frex* 2.0 with or without 100 ng of DNA were prepared as described above. After swelling, 2 μl of liposomes was diluted in 5.5 μl of feeding solution (see above) and incubated overnight at 37 °C in a BioRad C1000 Touch Thermal Cycler. Next, 1 μl of liposome mixture was diluted in 299 μl of isotonic buffer (20 mM HEPES, 180 mM potassium glutamate, 14 mM magnesium acetate, pH 7.6). Of the diluted liposome solution, 200 μl was injected in a BD FACSCelesta flow cytometer (BD Biosciences). Fluorescence was acquired with the pre-set mCherry (for Texas red) and GFP (for YFP) channels. Data was analysed using MATLAB and the online Cytobank application (https://community.cytobank.org/cytobank/experiments). The YFP versus Texas Red fluorescence intensity scatter plot was compared to the expected correlation between the signals of a lumen dye and a membrane dye assuming basic geometrical considerations. Let assume a population of spherical and unilamellar vesicles. Let also assume that both the YFP and the Texas Red dyes are randomly distributed inside the lumen (following a Poisson distribution) or in the membrane of liposomes, respectively. Using simple scaling geometrical factors, one obtains:

$$I_{\mathrm{YFP}} \propto \frac{4}{3}\pi r^3 \tag{6}$$

$$I_{\mathrm{TexasRed}} \propto 4\pi r^2 \tag{7}$$

where, r is the liposome radius, I_{YFP} and I_{TexasRed} are the fluorescence intensities in the YFP and Texas Red channels, respectively. Rearranging to eliminate the dependency with respect to r and linearizing on a logarithmic scale, one obtains:

$$\log\left(I_{\mathrm{YFP}}\right) = 1.5\,\log\left(I_{\mathrm{TexasRed}}\right) + \text{constant}. \tag{8}$$

This theoretical correlation was compared to actual fluorescence intensity data. Note that I_{YFP} represents the integrated intensity of YFP in a given liposome and cannot be compared to the mean YFP intensity inferred from confocal images.

Bulk gene expression kinetics

Bulk gene expression kinetics were measured with a spectrophotometer (Cary Eclipse from Agilent, exc/em 515/528 nm). PURE system reactions with 5 ng μl^{-1} (7.4 nM) of the *yfp* construct were assembled according to the manufacturers' instructions. When indicated, the *Cx43* DNA template was added at a final concentration of 6.25 ng μl^{-1} by substituting the equivalent volume of milliQ water. Samples were immediately transferred to 20 μl cuvettes (Hellma) and loaded into the spectrometer sample holder, preheated to 37 °C. Fluorescence intensity was converted into YFP concentration using a previously determined conversion factor [11].

Polyacrylamide gel electrophoresis

PURE*frex* reaction mixtures containing either or both *yfp* and *Cx43* DNA constructs (same concentrations as indicated for bulk kinetics and liposome experiments) were supplemented with 0.5 μl BODIPY-Lys-tRNA$_{\mathrm{Lys}}$ (FluoroTect™ GreenLys, Promega), an *in vitro* translation labelling system. The sample was incubated for 3 h at 37 °C, denatured for 10 min at 90 °C and analysed on a 12% SDS-PAGE using a fluorescence gel imager (Typhoon, Amersham Biosciences).

Results

High-throughput quantitative imaging of gene expression in individual liposomes smaller than ten micrometer reveals stochastic enhancement compared to bulk reactions

We first challenged requirement (ii) (see Introduction) by preparing bacterial cell-sized liposomes containing a mixed lipid composition comprising PC, PE, PG and cardiolipin phospholipids. Micrometer glass beads were used as a support for the lipid film to increase the total surface area and improve the yield of liposome production by natural swelling. The addition of rhamnose in the interspace between the stacked bilayers, combined with the presence of PEG-conjugated lipids, facilitate the osmotically driven flow of the aqueous solution into the lipid film, resulting in a high yield of unilamellar liposomes even in physiological buffers with a high ionic strength. Liposomes encapsulating PURExpress, PURE*frex* or PURE*frex*2.0, along with a linear DNA construct coding for the fluorescent reporter protein YFP, were produced. Gene expression was triggered by rising the temperature, and both the liposome membrane and synthesized YFP were imaged by LSCM.

Tens to hundreds of liposomes can be visualized in single fields of view, resulting in >10 000 vesicles per chamber even after 16 h incubation at 37 °C (figure 1(a), supplementary movie). Liposomes of various morphologies and sizes are observed. While many vesicles are unilamellar, a significant fraction of multivesicular and multilamellar liposomes are also generated. Most liposomes have a diameter below 10 μm, satisfying the size criteria that we formulated above. Notably, liposomes encapsulating PURE*frex* or PURE*frex*2.0 are on average larger than those containing PURExpress (mean/median radii are 2.3/2.0 μm, 2.6/2.1 μm and 1.8/1.5 μm, respectively) (figure 1(c)).

We then examined the activity of the PURE systems by imaging YFP fluorescence after overnight expression. We applied an image analysis script to automatically

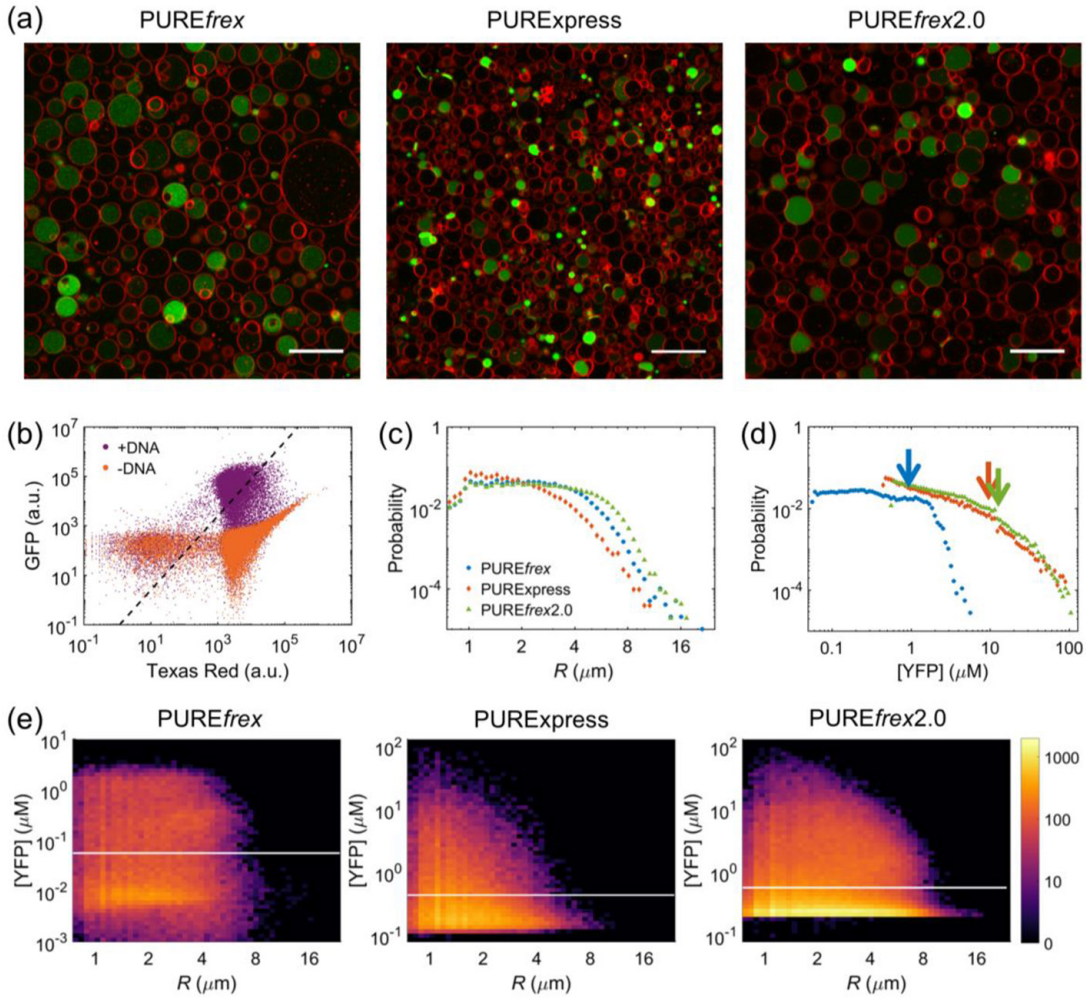

Figure 1. Confocal microscopy reveals stochastic enhancement of YFP expression in cell-sized vesicles. (a) Confocal micrographs of representative populations of liposomes (membrane in red) expressing YFP (green) in the three commercially available PURE systems. A higher laser power was used for PURE*frex*, to compensate for the lower YFP signal. Scale bars are 20 μm. (b) Scatter plot of flow cytometry measurements of Texas Red and YFP fluorescence for liposomes containing PURE*frex* 2.0 with (purple) and without (orange) *yfp* DNA. The appended dashed line with slope 1.5 represents the theoretical relationship between YFP and Texas Red signals in compliance with the assumptions used to derive equation (8). YFP-expressing liposomes correspond to the distinct purple cloud that appears in the +DNA sample. (c) Probability histogram of liposome radii (R) for PURE*frex* ($N = 96\,924$), PURExpress ($N = 102\,333$) and PURE*frex*2.0 ($N = 209\,870$), each from six independent microscopy experiments. (d) Probability histogram of YFP concentrations for the liposome populations displayed in (c). Arrows indicate the corresponding bulk YFP yield [11]. The low-concentration limit for PURExpress and PURE*frex*2.0 is shifted to higher concentration values compared to PURE*frex* as a consequence of the lower laser power applied. (e) Heat maps of YFP concentration versus liposome radius for the three liposome populations shown in (d). White horizontal lines indicate the YFP concentration threshold above which liposomes are considered expressing, i.e.: 56.2 nM for PURE*frex*, 437 nM for PURExpress and 573 nM for PURE*frex*2.0. The color scale indicates the number of liposomes. Note that graphs are displayed with logarithmic scales in (c)–(e).

identify the liposome lumina and to quantify the amount of synthesized active YFP after converting the average lumen intensity into protein concentration (figure S2). In all three PURE systems, about 30% of liposomes exhibit gene expression (determined as the signal above an intensity threshold, see Methods). Histograms of YFP concentration reveal a high liposome-to-liposome heterogeneity with all three PURE system variants (figure 1(d)). The mean/median concentration values are 0.5/0.3 μM, 3.5/1.7 μM and 2.6/1.1 μM for PURE*frex*, PURE*frex*2.0 and PURExpress, respectively. Interestingly, the distributions display a long tail with a fraction of liposomes outperforming the corresponding reaction in bulk (PURE*frex*: 5% with YFP > 1 μM, PURE*frex*2.0: 1.9% with YFP > 11 μM, PURExpress: 2% with YFP > 8.5 μM). Heat maps of YFP concentration plotted against liposome radius indicate no obvious relationship in PURE*frex* and PURE*frex*2.0 within the range of sizes analyzed (figure 1(e)). In PURExpress, liposomes with a diameter $\leqslant 3$ μm seem to show higher expression levels but the trend is not prominent (figure S3).

To obtain further quantitative insights about the number of YFP-expressing liposomes and sample heterogeneity, we performed flow cytometry measurements [41]. Using PURE*frex*2.0, we found that the amount of end-point expressing liposomes per microliter of swelling solution was ~75 000, corresponding to a concentration of 7.5×10^7 active vesicles ml^{-1} (figure 1(b)). Thus, the number of expressing

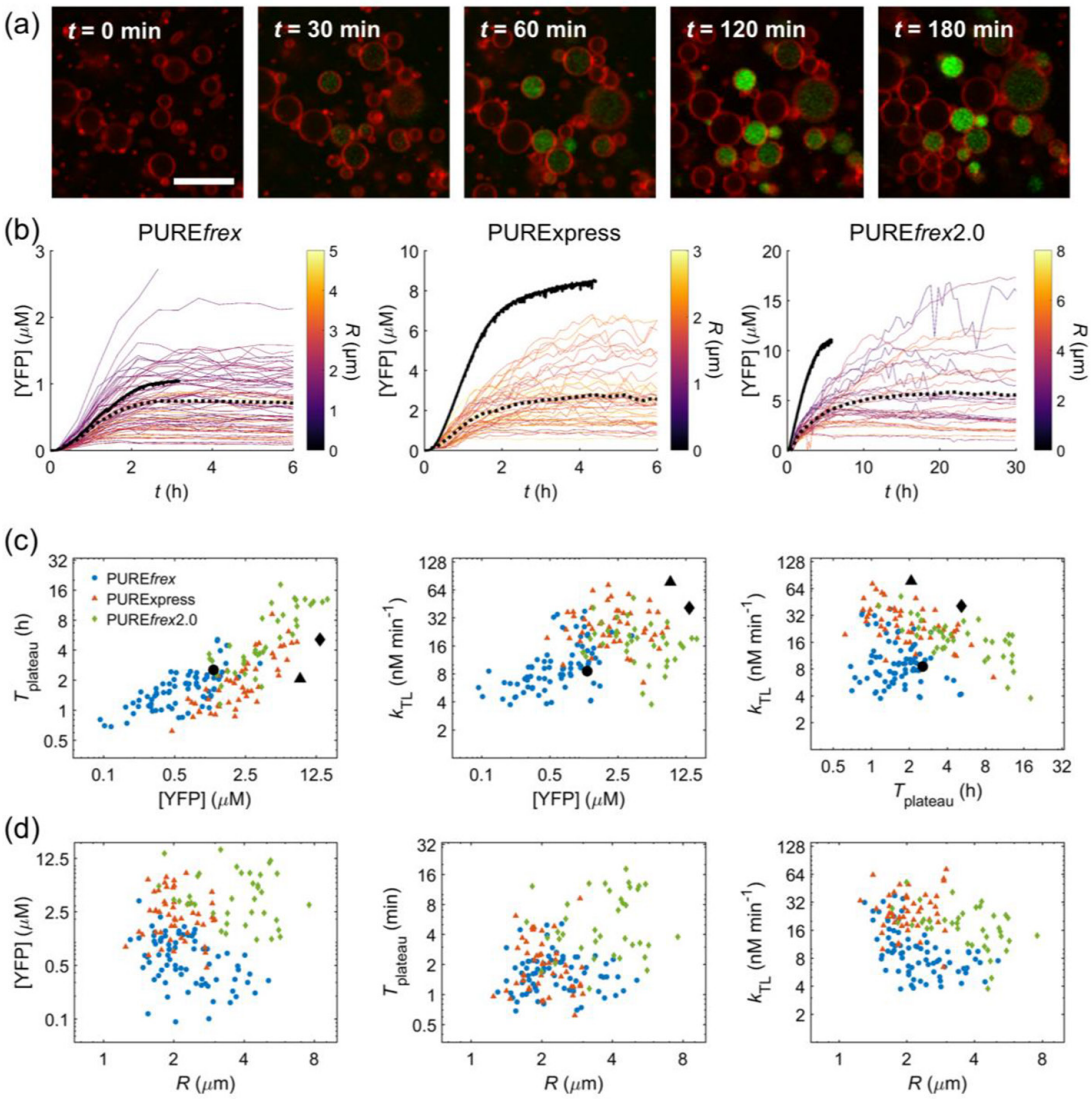

Figure 2. YFP concentration kinetics reveal heterogeneity in both expression lifespan and translation rate. (a) Timelapse microscopy images of PURE*frex*-containing liposomes producing YFP at 37 °C. Scale bar is 10 μm and scale is identical in all frames. Some vesicles sedimented onto the glass surface in the time course of imaging. (b) Time traces of YFP concentration for PURE*frex* ($N = 74$), PURExpress ($N = 49$), and PURE*frex*2.0 ($N = 38$), each from two independent experiments. Kinetic curves are color-coded with respect to the liposome radius R as indicated by the color bar. The black solid lines show the corresponding bulk gene expression kinetics. The dotted lines represent the average of the displayed liposome kinetics. (c) Scatter plots of final YFP concentration, expression lifespan $T_{plateau}$, and apparent translation rate k_{TL}, for the three PURE systems. Similar black symbols show the corresponding values from bulk expression kinetics. Parameters are determined by fitting a phenomenological model (see methods). (d) Scatter plots of fitted parameters from (c), versus the radius R of the liposome. Color coding is the same as in (c). Note that logarithmic plots are shown in (c) and (d) to better visualize the spread of parameter values.

liposomes per imaging chamber is ~150 000. In equation (8), we derived the expected relationship between the YFP (volume marker) and Texas Red (membrane marker) fluorescence intensity values assuming simple geometrical and dye partitioning constrains. Accordingly, a regression line with slope 1.5 (representing the volume-to-surface scaling factor of a sphere) was calculated and displayed on the fluorescence scatter plot shown in figure 1(b). The spread orthogonal to this line corresponds to the extent of heterogeneity, or uncorrelated variation, with respect to theoretical predictions. For instance, data points with $\frac{\Delta\log(I_{YFP})}{\Delta\log(I_{TexasRed})} < 1.5$ may correspond to multilamellar or elongated vesicles. The results show strong uncorrelated variation of the YFP-Texas Red paired signals, consistent with the observation that liposomes of similar sizes display YFP concentrations that can span up to two orders of magnitude (figures 1(d) and (e)).

Single-vesicle gene expression kinetics reveal dynamic heterogeneity

Next, we asked whether the large heterogeneity in the end-point protein synthesis yield is related to differences in the apparent translation rate or expression lifespan [11]. We performed time-lapse LSCM and tracked the fluorescence intensity of YFP inside individual liposomes (figure 2(a)). Fluorescence time traces exhibit similar qualitative behavior as bulk reaction kinetics: an initial time lag, a linear regime with constant slope representing the

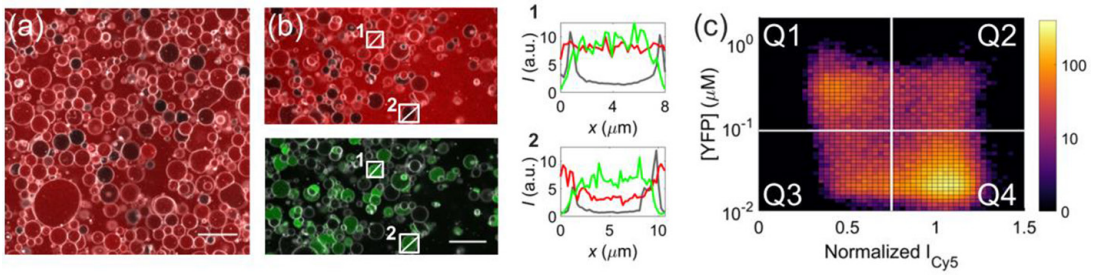

Figure 3. A significant fraction of YFP-expressing PURE*frex* liposomes shows spontaneous permeability to Cy5. (a) Fluorescence micrograph of a population of liposomes (membrane in white) with no encapsulated DNA. The Cy5 molecule (red) was added after liposome formation. Scale bar is 20 μm. (b) Microscopy images of liposomes (white) expressing YFP (green, bottom panel), with Cy5 (red, top panel) added after liposome formation. Scale bar is 20 μm. Line profiles of fluorescence intensity for the two liposomes highlighted: in grey the membrane signal, in red Cy5 and in green YFP. Arbitrary unit (a.u.). (c) Heat map of background-normalized Cy5 signal versus YFP concentration generated from 43 438 liposomes from one experiment. Color coding represents the number of liposomes. The white horizontal line corresponds to a YFP concentration threshold of 90 nM. The vertical white line corresponds to a normalized Cy5 intensity value of 0.75, which is defined as the threshold above which liposomes are considered filled with Cy5 and classified as permeable. Heat maps of four independent repeats are shown in figure S4.

apparent translation rate and a saturation phase with plateauing (figure 2(b)). Using phenomenological fitting, the apparent plateau time, translation rate and final yield of all individual kinetics were determined, their correlations analyzed and their values compared to bulk measurements (figure 2(c)). For all three parameters, a large variability is observed within each PURE system condition. Expression times vary from ~45 min up to 4 h with both PURE*frex* and PURExpress, in analogy with bulk observations. In PURE*frex*2.0 prolonged translation times up to 20 h were measured, which is significantly longer than in bulk reactions (~4 h). Expression duration and YFP yield are found to be strongly correlated in all PURE systems ($\rho = 0.60$, 0.77 and 0.73 for PURE*frex*, PURE*frex*2.0 and PURExpress, respectively), meaning that longer-lived expression reactions lead on average to a higher yield of YFP. The apparent translation rate is also subject to large variability, with values ranging from ~4 nM min^{-1} to >30 nM min^{-1}. Higher values are observed in PURExpress but they remain on average lower than in bulk reactions. Apparent translation rate and YFP yield are slightly correlated ($\rho = 0.40$) for PURE*frex*, but not for PURExpress and PURE*frex*2.0. For the latter two PURE system variants, the apparent translation rate and the time to reach plateau are negatively correlated ($\rho = -0.62$ and -0.49, respectively), indicating that reactions with faster protein production cease earlier on average. No marked size dependence can be observed (figure 2(d)).

These results clearly underline the dynamical diversity of liposome-confined gene expression as a manifestation of the unique environment conferred by every single vesicle. Quantitative inspection of the kinetics parameters reveals that the factors governing protein synthesis are different for the three types of PURE systems. Yet the causes limiting gene expression might differ between in-liposome and bulk reactions, in particular with PURE*frex*2.0 and PURExpress (figure 2(c)).

Differences in liposome permeability contribute to functional heterogeneity

Compositional diversity with regard to the copy number of DNA molecules and PURE system constituents are certainly factors contributing to the heterogeneity of gene expression in femtoliter liposomes. Another possible source of such a functional variability is the permeability state of the liposome membrane. We tested this hypothesis using PURE*frex*, as an extension of the detailed investigation of bulk reactions with this kit [11]. We first carried out a permeability assay using the Cy5 dye. It has a higher molecular mass than amino acids and nucleoside triphosphates but lower than any macromolecules in the PURE system. Therefore, it is a relevant fluorescent indicator of the permeability of low-molecular weight nutrients. The dye was supplied in the external solution, such that a fluorescence signal detected in the liposome lumen would reflect permeability across the lipid bilayer. No DNA was included in these experiments. We found that ~20% ± 6% (mean ± standard deviation, $n = 2$) of the liposomes do not contain the Cy5 dye and are thus impermeable (figure 3(a)). The same experiment was conducted with the *yfp* gene added (figures 3(b) and (c)). Combining the Cy5 signal (membrane permeability indicator) with the YFP fluorescence (gene expression reporter) and plotting the paired intensity values for every liposome on a heat map with four quadrants (Q1 impermeable/expressing, Q2 permeable/expressing, Q3 impermeable/nonexpressing and Q4 permeable/nonexpressing) reveal that ~40% of the expressing liposomes are impermeable (11% of the 29%), whereas only 16% of the nonexpressing liposomes are impermeable (11% of 71%) (figure 3(c)). Said differently, 51% of the impermeable liposomes are expressing (11% of the 28%), whereas only 23% of the permeable liposomes are expressing (17% of the 77%). Within the expressing liposome category, no clear difference in the final YFP yield between the permeable and impermeable vesicles can be observed

(figure 3(c)). Moreover, we did not find evidence for a correlation between liposome radius and permeability state.

Expression of the pore-forming protein connexin-43 increases the fraction of permeable liposomes

We cannot exclude the possibility that the liposomes classified as nonexpressing (~70% of the population) do actually enclose an active gene expression machinery but the concentration of synthesized YFP is too low for accurate detection (<103 nM). We reasoned that the functional expression and membrane incorporation of a pore-forming protein enabling the influx of the Cy5 dye (~790 Da) would provide a more sensitive readout. We chose the connexin-43 (Cx43) to stably permeabilize the liposome membrane [17]. We first validated the production of full-length Cx43 in a single-gene reaction or together with a second linear DNA coding for the YFP (figure 4(a)). Compartmentalized expression of the *Cx43* gene significantly reduces the number of Cy5-impermeable liposomes from ~22% (figure 3(a)) to less than 5% (figure 4(b)). This result indicates that a large fraction (~80%) of liposomes that are impermeable in the absence of pore-forming proteins can express the active Cx43, which elicits the uptake or efflux of permeable compounds along their concentration gradient. This percentage is significantly larger than the one calculated based on the correlation between the YFP and Cy5 signals, for which only 51% of the impermeable vesicles are found to express (figure 3(c)). This finding suggests the higher sensitivity of the Cx43-mediated uptake of a membrane-impermeable dye to probe gene expression activity in liposomes. Alternatively, the observation that a higher fraction of impermeable liposomes contains an active PURE system might be specific to Cx43 production and induced permeability, whereas individual *yfp* gene expression would be less effective in closed vesicles.

Functional expression of connexin-43 leads to membrane permeabilization without compromising YFP yield

Cx43-based gain-of-permeability was applied in combination with co-expression of the *yfp* gene to probe the influence of resource sharing and passive molecular diffusion across a protein channel on the IVTT performance. First, the bulk expression kinetics of active YFP were monitored with or without the Cx43-coding DNA template. Co-expression of the *Cx43* gene reduces the YFP final yield by ~40% (figure 4(c)), supporting the idea that some factors limiting productivity are common to the expression of the two genes (e.g. the concentration of translation initiation or elongation factors) and do not exclusively rely on the specific nucleotide or amino acid sequence. In contrast, the production period is not markedly affected (figures 2(b) and 4(h)). We next performed co-expression experiments with the *Cx43* and *yfp* genes inside liposomes. Given the bulk DNA concentrations (7.4 nM and 7.7 nM for the YFP- and Cx43-coding constructs, respectively) and assuming a Poisson distribution of DNA copies between liposomes, one expects on average ~150 DNA molecules of each gene inside a spherical liposome of 4 μm in diameter (volume 33.5 fl). This means that the probability for a liposome of that size to not contain at least one copy of each gene is negligible, even if one considers that only 10% of the DNA pool is transcriptionally active [23]. For smaller liposomes with a diameter of 2 μm, this probability increases to ~0.3 assuming 10% of active genes. Therefore, in the majority of liposomes, competition for nutrients and machinery is expected in order to produce both the YFP and Cx43 proteins.

Co-expressing *Cx43* and *yfp* genes within liposomes leads to a notable increase of the fraction of permeable liposomes (~72% without and ~95% with Cx43) (figures 3(c), 4(b) and (d)–(f)), similarly as observed with the sole expression of the *Cx43* gene (figures 3(a) and 4(b)). This finding suggests that sharing the IVTT resources for YFP production does not compromise the PURE system's ability to generate membrane-permeabilizing Cx43 pores. On the other hand, co-expression of the Cx43 protein results only in a slight increase of YFP-producing liposomes (~30% without and ~37% with Cx43) (figures 3(c) and 4(e)), and the histograms of YFP concentration are similar with and without Cx43 co-synthesis (figure 4(g)). Together these results suggest that, in contrast to bulk reactions, sharing of resources does not limit expression of YFP in liposomes. Alternatively, other mechanisms could compensate for a possible loss of production due to resource sharing. For example, Cx43-mediated molecular permeability might ensure continuous supply of nutrients that would otherwise be depleted, while avoiding lethal accumulation of reaction byproducts in sealed liposomes.

To test whether the translation rate or/and the protein synthesis lifespan could be increased upon selective membrane permeability, we measured the kinetics of YFP expression with both *yfp* and *Cx43* genes concurrently expressed (figure 4(h)). No differences were observed compared to individual YFP expression experiments (figure 4(i)), ruling out the hypothesis that Cx43 functional insertion into the membrane could lead to prolonged gene expression in PURE*frex*.

Time course analysis of the fluorescent permeability indicator reveals distinct mechanisms causing liposome membrane permeability

To gain some insights on the time evolution of membrane permeability, we tracked the Cy5 fluorescence signal inside individual liposomes expressing both *yfp* and *Cx43* genes or solely *yfp*. In particular, we wondered whether the type of permeability induced by Cx43 differs from that occurring in the absence of a specialized protein channel. Different typical time profiles were

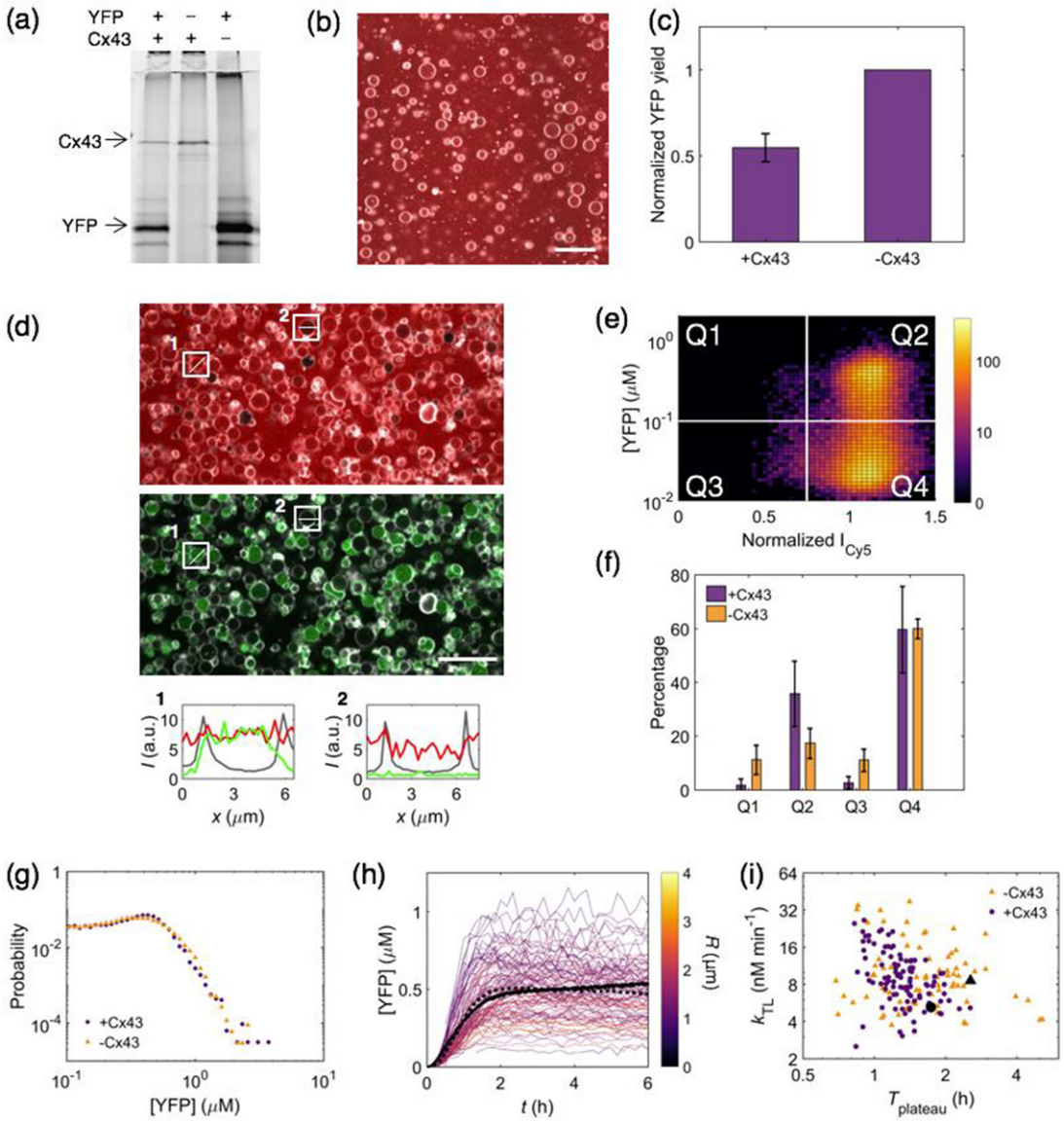

Figure 4. Co-expression of connexin-43 and YFP increases membrane permeability without compromising YFP yield. All experiments were performed with PURE*frex*. (a) SDS-PAGE GreenLys gel of individually expressed or co-expressed YFP and Cx43 proteins. (b) LSCM image of liposomes (white) encapsulating PURE*frex* and *Cx43* DNA. The Cy5 dye (red) was added after liposome formation. Scale bar is 20 μM. (c) YFP expression yield obtained at the plateau of bulk reactions in the presence of *Cx43* DNA, normalized to the end-point yield obtained in a minus *Cx43* DNA bulk reaction conducted in parallel. Data are the average of two experiments, with error bar representing standard deviation. (d) LSCM images of liposomes (membrane in white) encapsulating the *yfp* and *Cx43* genes. Both the Cy5 intensity (red, top panel) and YFP (green, bottom panel) signal were acquired simultaneously. Line profiles correspond to liposomes highlighted in the micrographs. (e) Heat map of normalized Cy5 signal versus YFP concentration for 39 046 liposomes from one experiment. Color coding represents the number of liposomes. The white horizontal line corresponds to a YFP concentration of 103 nM, above which liposomes are considered expressing. The vertical white line corresponds to a normalized Cy5 intensity value of 0.75, the threshold above which liposomes are considered filled with Cy5. Heat maps of two independent repeats are shown in figure S4. (f) Mean fraction of liposomes in each quadrant, as indicated in (e), both in the presence (three independent repeats) and absence (five independent repeats, figures 3(c) and S4) of Cx43. Error bar represents standard deviation. (g) Probability histogram of YFP concentration in the presence ($N = 84\,260$) and absence ($N = 112\,989$) of Cx43. Logarithmic scales are displayed. (h) Time traces of YFP concentration for 100 liposomes containing YFP and Cx43 DNA. Color coding represents liposome radius R. Black line indicates bulk kinetics and the dotted line is the average of the displayed liposome kinetics. (i) Scatter plot of expression lifespan T_{plateau} versus the apparent translation rate k_{TL}, as determined by fitting the time traces in (h) to a phenomenological model (purple symbols). The appended orange symbols correspond to PURE*frex* data shown in figure 2. Black symbols are data from bulk experiments (c). Logarithmic scales are displayed.

monitored, which can each be associated with a certain permeability state of the membrane (figure 5(a)): (Phenotype I) Liposomes do not entrap Cy5 at the start of the kinetics and remain empty, indicating that the membrane is impermeable throughout the measurement period. (Phenotype II) Liposomes exhibit Cy5 signal that photobleaches at the same rate as the background (Cy5 in the outside solution), suggesting continuous membrane permeability. (Phenotype III) Liposomes initially contain Cy5 that photobleaches faster than the background signal, suggesting that the dye cannot freely exchange across

the membrane. This category is more populated in liposomes that do not express YFP, hence likely not Cx43 (figure 5(c)). (Phenotype IV) Liposomes experience a sudden increase of Cy5 intensity at $t = t^*$ (figure 5(b)), after which bleaching occurs similarly as the background signal. This phenotype is most predominant in YFP-expressing liposomes with the encapsulated *Cx43* gene (figure 5(c)). Therefore, we attribute this behavior to the internal biosynthesis and functional assembly of stable Cx43 pores. Furthermore, t^* values are distributed around 60 min (figure 5(b)), a reasonable value for the expression and membrane insertion of the connexin pore. (Phenotype V) Liposomes display a sudden increase of Cy5 intensity at $t = t^*$, after which bleaching occurs at a faster rate than the background. Such transient permeability events occur randomly throughout the acquisition period (figure 5(b)) and may arise from unstable membrane defects. (Phenotype VI) This category encompasses Cy5 fluorescence time traces that cannot be classified in one of the previous phenotypes, for example due to multiple filling events or to a filling event occurring at $t > 300$ min, for which the distinction between phenotypes IV and V cannot be assessed.

Discussion

A milestone towards the realization of a synthetic minimal cell is to achieve robust gene expression inside liposomes, recapitulating cytoplasmic and membrane processes found in bacteria like *E. coli*. In the present study, we demonstrate the high-yielding production of cell-sized (<10 μm) liposomes expressing genes by an encapsulated transcription-translation machinery. Protein-synthesizing phospholipid vesicles are stable for at least 16 h and can be immobilized at high density on a glass surface to facilitate long-time, high-throughput fluorescence imaging at the single liposome level. Most publications on gene expression inside liposomes display images with only a few vesicles, with severe limitations on the ability to derive quantitative information with statistical relevance, in particular when it comes to identify rare phenotypes. The high-content liposome analysis described here enabled quantification of essential properties, such as the expression yield, apparent kinetic parameters, membrane permeability states, and revealed large vesicle-to-vesicle heterogeneity. Using flow cytometry as a complementary analytical technique [41], we estimated the concentration of gene-expressing liposomes (7.5×10^7 vesicles ml^{-1} with PURE*frex*2.0) and supported the uncorrelated variation in the amounts of expressed YFP and membrane dye. Regarding the protein synthesis yield and the apparent translation lifespan as measures of the IVTT system's performance, we recommend to utilize PURE*frex*2.0 for liposome-compartmentalized reactions. Furthermore, triggered membrane permeability was achieved by expressing the non-*E. coli* protein Cx43 that acts as a general diffusion pore.

Various liposome preparation methods have been described in the literature (recently reviewed in [42]): lipid film hydration [43] and its many variants (lipid-coated powder [44] or glass-bead [4] carriers, electroformation [45], hydrogel-based [46–48]), emulsion droplet-phase transfer [49–51], and microfluidic-based approaches [19, 52–57]. In particular, the water-in-oil emulsion transfer and microfluidic-assisted methods have recently gained popularity in the liposome community, largely because of their ability to generate monodisperse and unilamellar vesicles. However, a vast majority of them produce giant vesicles with a diameter >10 μm. While such big liposomes can easily be manipulated and imaged by standard optical microscopes, they might not provide a physiological environment when it comes to recapitulate cytoplasmic and membrane processes (e.g. the *E. coli*-based translation machinery of the PURE system) occurring in bacteria with a size of a few micrometer only. In fact, a number of geometrical cues are known to drive biological functions in living cells [58,59]: the volume and the actual copy number of biochemical reactants, surface-to-volume ratio which regulates the molecular diffusion across the membrane as well as protein and RNA interactions with the lipid surface, confinement effects that influence biochemical reactions as a function of the order of the reaction, macromolecular crowding that is more prominent in small liposomes [28], and membrane curvature that affects lipid sorting and membrane protein functions [60].

Moreover, microfluidics and water-in-oil droplet phase transfer methods to form liposomes employ mineral oil or organic solvent that may remain in the form of residual traces in the hydrophobic core of the bilayer [52, 61, 62]. This may lead to altered membrane characteristics, such as lateral diffusion and flip-flop of lipids, microdomain formation, mechanical properties, permeability and biological activity of membrane-embedded proteins [42, 51]. Actually, in the vast majority of the microfluidics-based vesicle formation studies, the possible presence of residual amounts of oil or solvent (not visible pockets) is not examined, despite the proven analytical efficacy of Raman spectroscopy and microscopy techniques [19, 61]. In contrast, our glass bead-assisted natural lipid film swelling approach ensures unaltered membrane properties, which is essential to equip liposomes with more elaborate membrane-dependent functionalities. As a trade-off, however, a significant fraction of the liposomes generated with the present method are multilamellar or multivesicular, and the vesicle size distribution is polydisperse (figure 1), which complicates fully automated image analysis and discards lipids in nonfunctional liposomes. This caveat is mitigated if one considers the large number of gene-expressing liposomes and the opportunity offered by such a heterogeneity. Indeed, in a single sample, a large combinatorial space of molecular inputs and geometrical

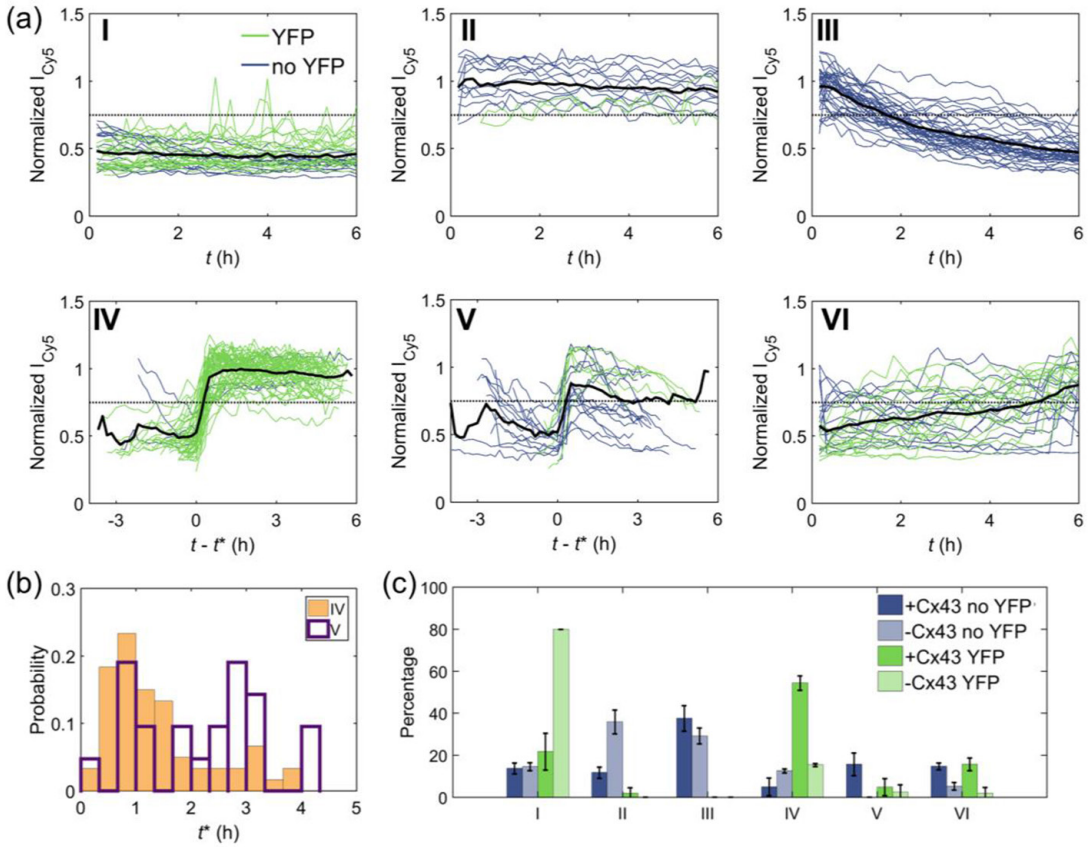

Figure 5. Expression of Cx43 inside liposomes leads to a specific permeability time profile. (a) Time traces of normalized Cy5 signal in liposomes expressing (green, $N = 100$) or not expressing (blue, $N = 100$) YFP, from two independent experiments. In both conditions, the *Cx43* gene was co-encapsulated. Black solid lines indicate average time traces. Dotted horizontal lines depict the Cy5 permeability threshold. Phenotypes, as indicated by roman numerals, are described in the main text. For IV and V, a time shift t^* is applied to align curves based on the occurrence of the filling event. (b) Probability histogram of t^* values, for phenotypes IV ($N = 60$ liposomes) and V ($N = 21$). (c) Occurrence of phenotypes, as percentage of the total number of time traces, for experiments with *Cx43* DNA (shown in a) and without (figure S5). Error bars represent standard deviation between experiments. In total 400 traces were analysed, 100 for each of the four conditions.

parameters can be explored, increasing the likelihood to find liposomes exhibiting desired features, e.g. expression kinetics or vesicle morphology.

Our work shows that confinement of gene expression in femtoliter liposomes leads to higher heterogeneity of the apparent kinetic parameter values compared to bulk reactions (figure 2 and accompanying article [11]). It is unclear whether the inhibitory mechanisms unraveled in bulk measurements similarly affect protein synthesis in liposome-confined reactions. The compositional heterogeneity and low-copy number effects arising from the stochastic entrapment of PURE system constituents make every liposome unique. Hence, the parameters that control the dynamics of the network and govern its performance might differ from one liposome to the other. Note that the absolute number of macromolecules can on average be >100 (as calculated above for DNA molecules), yet the effective amount might be significantly lower if one considers partial inactivation [23], association with multiple partners into distinct complexes (e.g. translation factors, including tRNAs), or deviation from a Poisson encapsulation profile [28]. Intriguingly, a subset of liposomes express remarkably high protein concentration (figure 1(d)) or have a long translation lifespan (figure 2) surpassing the performance of any of the bulk reactions that we monitored so far [11]. These exceptional properties certainly result from peculiar initial conditions and membrane permeability state. Further studies should investigate the molecular determinants that confer such properties. For instance, individual PURE system constituents could be fluorescently labelled and their encapsulation profile correlated with gene expression properties. The presence of distinct liposome sub-populations with permeable or impermeable membrane to small charged solutes has already been reported, albeit with a different lipid composition and liposome formation protocol [63]. Probing membrane tension with a fluorescent lipid reporter [64] could unveil the mechanical and structural properties associated to the permeability of gene expressing liposomes. We propose that this heterogeneity should be exploited—instead of being seen as a drawback—e.g. by mapping in-liposome activity (amount of synthesized protein or expression kinetic parameters) as a function of the internal concentration of key components in one-pot reactions. This approach will aid the implementation of biological

subsystems whose functioning relies on a narrow range of initial conditions that would hardly be tractable in batch mode screening reactions.

Extending this work to achieve sustainable RNA and protein synthesis through continuous liposome feeding from externally supplied nutrients (i.e. creatine phosphate, nucleoside triphosphates, amino acids) will be an important milestone towards the creation of a semisynthetic minimal cell. Long-lived gene-expressing liposomes, as reported in one study with an *E. coli* cell lysate entrapped inside liposomes with membrane-embedded α-hemolysin pores [3], was not realized in PURE*frex* under the tested conditions (figures 4(h) and (i)). Next to the different type of membrane channels used in the two studies, it is likely that PURE*frex* reactions in the tracked liposomes are limited by other factors than shortage of low-molecular weight substrates or accumulation of inhibiting byproducts. This hypothesis is consistent with results obtained for PURE*frex* bulk reactions in a dialysis chamber [11]. Further developments of liposomes actively interfacing with their environment may take advantage of *in situ* expressed Cx43 to permit the entrance of membrane-impermeable molecules involved in transcriptional regulation, signaling, sensing or communication between liposomes.

Acknowledgments

We gratefully thank Zhanar Abil for assisting with flow cytometry experiments. We also thank Mees Kersbergen for contributing preliminary experiments, Katy Wei for deriving the correction factor when estimating liposome radius, Johannes Kattan for performing the protein gel, Miranda Visser for writing the kinetics analysis script, Jonás Noguera López for designing the glass chamber, Martin Depken for fruitful discussion on the vesicle size analysis, and Damien Baigl (ENS Paris) for providing us with plasmids containing the *Cx43* gene. Microscopy measurements were performed at the Kavli Nanolab Imaging Center Delft.

This work was financially supported by the Netherlands Organization for Scientific Research (NWO/OCW) through a VIDI grant (project number 723.012.007) to C D and the Frontiers of Nanoscience Program.

Author contributions

D B performed the experiments. P N trained D B in PURE system, liposome preparation and fluorescence imaging, and edited the manuscript. D B and C D designed experiments, analyzed data and wrote the manuscript.

Supporting information

The supplementary information is available on the journal website. It includes Supporting Text, supporting figures and a supporting movie.

ORCID iDs

Christophe Danelon https://orcid.org/0000-0002-0961-6640

References

[1] Luisi P L and Stano P (ed) 2011 *The Minimal Cell: the Biophysics of Cell Compartment and the Origin of Cell Functionality* 1st edn (Berlin: Springer)
[2] Nomura S M, Tsumoto K, Hamada T, Akiyoshi K, Nakatani Y and Yoshikawa K 2003 Gene expression within cell-sized lipid vesicles *ChemBioChem* **4** 1172–5
[3] Noireaux V and Libchaber A 2004 A vesicle bioreactor as a step toward an artificial cell assembly *Proc. Natl Acad. Sci. USA* **101** 17669–74
[4] Nourian Z, Roelofsen W and Danelon C 2012 Triggered gene expression in fed-vesicle microreactors with a multifunctional membrane *Angew. Chem., Int. Ed.* **51** 3114–8
[5] Scott A, Noga M J, de Graaf P, Westerlaken I, Yildirim E and Danelon C 2016 Cell-free phospholipid biosynthesis by gene-encoded enzymes reconstituted in liposomes *PLoS One* **11** e0163058
[6] Van Nies P, Westerlaken I, Blanken D, Mencía M, Salas M and Danelon C 2018 Self-replication of DNA by its encoded proteins in liposome-based synthetic cells *Nat. Commun.* **9** 1583
[7] Ichihashi N, Usui K, Kazuta Y, Sunami T, Matsuura T and Yomo T 2013 Darwinian evolution in a translation-coupled RNA replication system within a cell-like compartment *Nat Commun.* **4** 2494
[8] Sunami T, Ichihashi N, Nishikawa T, Kazuta Y and Yomo T 2016 Effect of liposome size on internal RNA replication coupled with replicase translation *Chembiochem* **17** 1282–9
[9] Shimizu Y, Inoue A, Tomari Y, Suzuki T, Yokogawa T, Nishikawa K and Ueda T 2001 Cell-free translation reconstituted with purified components *Nat. Biotechnol.* **19** 751–5
[10] Shimizu Y, Kanamori T and Ueda T 2005 Protein synthesis by pure translation systems *Methods* **36** 299–304
[11] Doerr A, de Reus E, van Nies P, van der Haar M, Wei K, Kattan J, Wahl A and Danelon C 2019 Modelling cell-free RNA and protein synthesis with minimal systems *Phys. Biol.* **16** 025001
[12] Saito H, Kato Y, Le Berre M, Yamada A, Inoue T, Yosikawa K and Baigl D 2009 Time-resolved tracking of a minimum gene expression system reconstituted in giant liposomes *Chembiochem* **10** 1640–3
[13] Sakamoto R, Noireaux V and Maeda Y T 2018 Anomalous scaling of gene expression in confined cell-free reactions *Sci. Rep.* **8** 7364
[14] Vogele K, Frank T, Gasser L, Goetzfried M A, Hackl M W, Sieber S A, Simmel F C and Pirzer T 2018 Towards synthetic cells using peptide-based reaction compartments *Nat. Commun.* **9** 3862
[15] Martino C, Kim S-H, Horsfall L, Abbaspourrad A, Rosser S J, Cooper J and Weitz D A 2012 Protein expression, aggregation, and triggered release from polymersomes as artificial cell-like structures *Angew. Chem., Int. Ed.* **51** 6416–20
[16] Nourian Z, Scott A and Danelon C 2014 Toward the assembly of a minimal divisome *Syst. Synth. Biol.* **8** 237–47
[17] Liu Y J, Hansen G P, Venancio-Marques A and Baigl D 2013 Cell-free preparation of functional and triggerable giant proteoliposomes *Chembiochem* **14** 2243–7
[18] Majumder S, Garamella J, Wang Y L, DeNies M, Noireaux V and Liu A P 2017 Cell-sized mechanosensitive and biosensing compartment programmed with DNA *Chem. Commun.* **53** 7349–52
[19] Kamiya K, Kawano R, Osaki T, Akiyoshi K and Takeuchi S 2016 Cell-sized asymmetric lipid vesicles facilitate the investigation of asymmetric membranes *Nat. Chem.* **8** 881–9

[20] Uyeda A, Nakayama S, Kato Y, Watanabe H and Matsuura T 2016 Construction of an *in vitro* gene screening system of the *E. coli* EmrE transporter using liposome display *Anal. Chem.* **88** 12028–35
[21] Kuruma Y, Stano P, Ueda T and Luisi P L 2009 A synthetic biology approach to the construction of membrane proteins in semi-synthetic minimal cells *Biochim. Biophys. Acta* **1788** 567–74
[22] Exterkate M, Caforio A, Stuart M C A and Driessen A J M 2018 Growing membranes *in vitro* by continuous phospholipid biosynthesis from free fatty acids *ACS Synth. Biol.* **7** 153–65
[23] Nourian Z and Danelon C 2013 Linking genotype and phenotype in protein synthesizing liposomes with external supply of resources *ACS Synth. Biol.* **2** 186–93
[24] Mavelli F, Marangoni R and Stano P 2015 A simple protein synthesis model for the PURE system operation *Bull. Math. Biol.* **77** 1185–212
[25] Lazzerini-Ospri L, Stano P, Luisi P L and Marangoni R 2012 Characterization of the emergent properties of a synthetic quasi-cellular system *BMC Bioinform.* **13** S9
[26] Caveney P M, Norred S E, Chin C W, Boreyko J B, Razooky B S, Retterer S T, Collier C P and Simpson M L 2017 Resource sharing controls gene expression bursting *ACS Synth. Biol.* **6** 334–43
[27] Nishimura K, Tsuru S, Suzuki H and Yomo T 2015 Stochasticity in gene expression in a cell-sized compartment *ACS Synth. Biol.* **4** 566–76
[28] Pereira de Souza T, Steiniger F, Stano P, Fahr A and Luisi P L 2011 Spontaneous crowding of ribosomes and proteins inside vesicles: a possible mechanism for the origin of cell metabolism *Chembiochem* **12** 2325–30
[29] Hansen M M, Meijer L H, Spruijt E, Maas R J, Rosquelles M V, Groen J, Heus H A and Huck W T 2016 Macromolecular crowding creates heterogeneous environments of gene expression in picolitre droplets *Nat. Nanotechnol.* **11** 191–7
[30] Norred S E, Caveney P M, Chauhan G, Collier L K, Collier C P, Abel S M and Simpson M L 2018 Macromolecular crowding induces spatial correlations that control gene expression bursting patterns *ACS Synth. Biol.* **7** 1251–8
[31] Okano T, Matsuura T, Suzuki H and Yomo T 2014 Cell-free protein synthesis in a microchamber revealed the presence of an optimum compartment volume for high-order reactions *ACS Synth. Biol.* **3** 347–52
[32] Van Nies P *et al* 2013 Unbiased tracking of the progression of mRNA and protein synthesis in bulk and in liposome-confined reactions *Chembiochem* **14** 1963–6
[33] Frazier J M, Chushak Y and Foy B 2009 Stochastic simulation and analysis of biomolecular reaction networks *BMC Syst. Biol.* **3** 64
[34] Altamura E, Carrara P, D'Angelo F, Mavelli F and Stano P 2018 Extrinsic stochastic factors (solute partition) in gene expression inside lipid vesicles and lipid-stabilized water-in-oil droplets: a review *Synth. Biol.* **3** ysy011
[35] Dezi M, Di Cicco A, Bassereau P and Lévy D 2013 Detergent-mediated incorporation of transmembrane proteins in giant unilamellar vesicles with controlled physiological contents *Proc. Natl Acad. Sci. USA* **110** 7276–81
[36] Kumar N M and Gilula N B 1996 The gap junction communication channel *Cell* **84** 381–8
[37] Van Nies P, Canton A S, Nourian Z and Danelon C 2015 Monitoring mRNA and protein levels in bulk and in model vesicle-based artificial cells *Methods Enzymol.* **550** 187–214
[38] Tsumoto K, Matsuo H, Tomita M and Yoshimura T 2009 Efficient formation of giant liposomes through the gentle hydration of phosphatidylcholine films doped with sugar *Colloids Surf.* B **68** 98–105
[39] Schindelin J *et al* 2012 Fiji: an open-source platform for biological-image analysis *Nat. Methods* **9** 676–82
[40] Ang J, Harris E, Hussey B, Kil R and McMillen D 2013 Tuning response curves for synthetic biology *ACS Synth. Biol.* **2** 547–67
[41] Sunami T, Sato K, Matsuura T, Tsukada K, Urabe I and Yomo T 2006 Femtoliter compartment in liposomes for *in vitro* selection of proteins *Anal. Biochem.* **357** 128–36
[42] Stein H, Spindler S, Bonakdar N, Wang C and Sandoghdar V 2017 Production of isolated giant unilamellar vesicles under high salt concentrations *Frontiers Physiol.* **8** 63
[43] Reeves J P and Dowben R M 1969 Formation and properties of thin-walled phospholipid vesicles *J. Cell. Physiol.* **73** 49–60
[44] Payne N I, Timmins P, Ambrose C V, Ward M D and Ridgway F 1986 Proliposomes: a novel solution to an old problem *J. Pharm. Sci.* **75** 325–9
[45] Angelova M I and Dimitrov D S 1986 Liposome electroformation *Faraday Discuss. Chem. Soc.* **81** 303
[46] Horger K S, Estes D J, Capone R and Mayer M 2009 Films of agarose enable rapid formation of giant liposomes in solutions of physiologic ionic strength *J. Am. Chem. Soc.* **131** 1810–9
[47] Weinberger A, Tsai F C, Koenderink G H, Schmidt T F, Itri R, Meier W, Schmatko T, Schröder A and Marques C 2013 Gel-assisted formation of giant unilamellar vesicles *Biophys J.* **105** 154–64
[48] López Mora N, Hansen J S, Gao Y, Ronald A A, Kieltyka R, Malmstadt N and Kros A 2014 Preparation of size tunable giant vesicles from cross-linked dextran (ethylene glycol) hydrogels *Chem. Commun.* **50** 1953–5
[49] Pautot S, Frisken B J and Weitz D A 2003 Engineering asymmetric vesicles *Proc. Natl Acad. Sci. USA* **100** 10718–21
[50] Abkarian M, Loiseau E and Massiera G 2011 Continuous droplet interface crossing encapsulation (cDICE) for high throughput monodisperse vesicle design *Soft Matter* **7** 4610–4
[51] Blosser M C, Horst B G and Keller S L 2016 cDICE method produces giant lipid vesicles under physiological conditions of charged lipids and ionic solutions *Soft Matter* **12** 7364–71
[52] Funakoshi K, Suzuki H and Takeuchi S 2007 Formation of giant lipid vesicle like compartments from a planar lipid membrane by a pulsed jet flow *J. Am. Chem. Soc.* **129** 12608–9
[53] Shum H C, Lee D, Yoon I, Kodger T and Weitz D A 2008 Double emulsion templated monodisperse phospholipid vesicles *Langmuir* **24** 7651–3
[54] Matosevic S and Paegel B M 2011 Stepwise synthesis of giant unilamellar vesicles on a microfluidic assembly line *J. Am. Chem. Soc.* **133** 2798–800
[55] Karamdad K, Law R W, Seddon J M, Brooks N J and Ces O 2015 Preparation and mechanical characterisation of giant unilamellar vesicles by a microfluidic method *Lab Chip* **15** 557–62
[56] Deshpande S, Caspi Y, Meijering A E and Dekker C 2016 Octanol-assisted liposome assembly on chip *Nat. Commun.* **7** 10447
[57] Deng N N, Yelleswarapu M and Huck W T 2016 Monodisperse uni- and multicompartment liposomes *J. Am. Chem. Soc.* **138** 7584–91
[58] Wingreen N S and Huang K C 2015 Physics of intracellular organization in bacteria *Annu. Rev. Microbiol.* **69** 361–79
[59] Govindarajan S, Nevo-Dinur K and Amster-Choder O 2012 Compartmentalization and spatiotemporal organization of macromolecules in bacteria *FEMS Microbiol. Rev.* **36** 1005–22
[60] Iversen L, Mathiasen S, Larsen J B and Stamou D 2015 Membrane curvature bends the laws of physics and chemistry *Nat. Chem. Biol.* **11** 822–5
[61] Kirchner S R, Ohlinger A, Pfeiffer T, Urban A S, Stefani F D, Deak A, Lutich A A and Feldmann J 2012 Membrane composition of jetted lipid vesicles: a Raman spectroscopy study *J. Biophoton.* **5** 40–6
[62] Van Swaay D and deMello A 2013 Microfluidic methods for forming liposomes *Lab Chip* **13** 752–67
[63] Nishimura K, Matsuura T, Sunami T, Fujii S, Nishimura K, Suzuki H and Yomo T 2014 Identification of giant unilamellar vesicles with permeability to small charged molecules *RSC Adv.* **4** 35224–32
[64] Colom A, Derivery E, Soleimanpour S, Tomba C, Molin M D, Sakai N, González-Gaitán M, Matile S and Roux A 2018 A fluorescent membrane tension probe *Nat. Chem.* **10** 1118–25